How to cite: *Angew. Chem. Int. Ed.* **2020**, *59*, 21510–21514
International Edition: doi.org/10.1002/anie.202010257
German Edition: doi.org/10.1002/ange.202010257

Supramolecular Chemistry

Exosome-Mimetic Supramolecular Vesicles with Reversible and Controllable Fusion and Fission**

Jie Li, Kang Peng, Youmei Li, Jianxing Wang, Jianbin Huang, Yun Yan, Dong Wang,* and Ben Zhong Tang**

Abstract: *The fusion and fission behaviors of exosomes are essential for the cell-to-cell communication. Developing exosome-mimetic vesicles with such behaviors is of vital importance, but still remains a big challenge. Presented herein is an artificial supramolecular vesicle that exhibits redox-modulated reversible fusion-fission functions. These vesicles tend to fuse together and form large-sized vesicles upon oxidation, undergo a fission process and then return to small-sized vesicles through reduction. Noteworthy, the aggregation-induced emission (AIE) characteristics of the supramolecular building blocks enable the molecular configuration during vesicular transformation to be monitored by fluorescence technology. Moreover, the presented vesicles are excellent nanocarrier candidates to transfer siRNA into cancer cells.*

Exosomes refer to the nanosized extracellular vesicles that are closely related to intercellular signaling and substances transport.[1] A fission process of releasing new vesicles from one cell and a fusion process of swallowing by another cell are normally involved during cell-to-cell communication, and such two processes are generally reversible and controllable in living organelles.[2] However, the knowledge on membrane behaviors of fusion and fission processes, as well as their modulating factors still remains sparse due to the complex composition of exosomes and cellular environment.[3] This obstacle inspires the development of artificial vesicles that possess similar architecture and fission-fusion behaviors as exosomes to serve as models. Despite the actual components and behaviors of artificial vesicles are different from cellular membranes, artificial vesicles have been widely accepted as excellent cellular membrane model to mimic the structure and behaviors of cells or subcellular organelles.[4] Therefore, the exosome-mimetic artificial vesicles could provide possibilities for fundamental understanding of fission-fusion processes of exosomes, and open new practical applications as delivery in biosystems.[5]

Great progresses have been made on design and creation of artificial vesicles with fusion or fission behaviors, however, these are always one-way transformations.[4] To the best of our knowledge, there have been no previous reports on utilization of artificial vesicles to mimic the reversible and controllable fusion and fission behaviors of exosomes. In most cases, the fusion or fission processes are extensively driven by chemical reactions or osmotic stress.[6] The chemical reactions and osmotic stress offers sufficient energy to change surface tension of membrane and water volume inside vesicles, generating the subsequent morphological transformations. However, the reversible transformation is difficult to be realized, mainly because these chemical reactions are irreversible and few approaches can be explored to decrease osmotic stress outside vesicles back to original state. Evidently, the exploration of artificial vesicles with reversible and controllable fusion and fission behaviors as exosomes is a definitely appealing yet significantly challenging task.

Inspired by the reversibility of redox reaction, herein, we fabricated a novel Fe^{2+}-coordinated supramolecular vesicle, which demonstrated the reversible fusion and fission behaviors modulated by redox treatments. As illustrated in Scheme 1, the vesicle underwent a fusion process upon oxidation of Fe^{2+} to Fe^{3+}, while a fission process further proceeded when Fe^{3+} was reduced to Fe^{2+}. Noteworthy, aggregation-induced emission (AIE) active molecules were used as building blocks, allowing us to monitor the molecular configuration during vesicular transformation via fluorescence technology.[7] Moreover, these vesicles can serve as

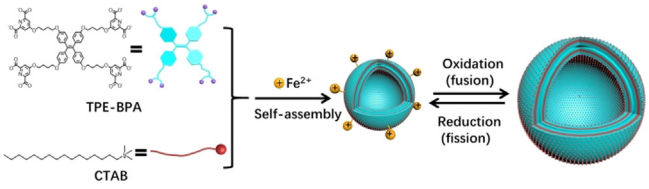

Scheme 1. Schematic illustration of construction of exosome-mimetic vesicles, and their reversible and controllable fusion-fission behaviors.

[*] Dr. J. Li, Dr. Y. Li, Dr. J. Wang, Prof. D. Wang
Center for AIE Research, Shenzhen Key Laboratory of Polymer Science and Technology, College of Materials Science and Engineering, Shenzhen University, Shenzhen 518060 (China)
E-mail: wangd@szu.edu.cn
Dr. J. Li, Dr. Y. Li, Dr. J. Wang
Key Laboratory of Optoelectronic Devices and Systems of Ministry of Education and Guangdong Province, College of Physics and Optoelectronic Engineering, Shenzhen University
Shenzhen 518060 (China)
Dr. J. Li, K. Peng, Prof. J. Huang, Prof. Y. Yan
Beijing National Laboratory for Molecular Sciences (BNLMS), College of Chemistry and Molecular Engineering, Peking University
Beijing 100871 (China)
E-mail: yunyan@pku.edu.cn
Prof. B. Z. Tang
Department of Chemistry, The Hong Kong University of Science and Technology, Clear Water Bay, Kowloon, Hong Kong (China)
E-mail: tangbenz@ust.hk

[**] A previous version of this manuscript has been deposited on a preprint server (https://doi.org/10.26434/chemrxiv.12408173.v1).

Supporting information and the ORCID identification number(s) for the author(s) of this article can be found under: https://doi.org/10.1002/anie.202010257.

nanocarriers to transfer siRNA into cancer cells. This study presents an important step forward toward the development of artificial cellular membrane.

The Fe^{2+}-coordinated vesicles were constructed by self-assembly of AIE-active TPE-BPA, cetyltrimethylammonium bromide (CTAB) and Fe^{2+} ions (Scheme 1). TPE-BPA was a negative charged tetra-armed molecule, which exhibited strong fluorescent emission in aggregated states. It was able to spontaneously self-assemble into neutral fluorescent vesicles through integrating with eight positively charged CTAB molecules via ionic interaction.[8] TPE-BPA also carried coordinating heads, making the TPE-BPA@8CTAB supramolecular vesicles capable to coordinate with many metal ions, such as Fe^{2+} and Fe^{3+}.[9] It was observed that with continuously adding Fe^{2+} ions into TPE-BPA@8CTAB vesicles solution, the Zeta potentials and UV absorption of coordinating heads (257 nm) remarkably increased and reached a platform at the molar ratio of TPE-BPA/Fe^{2+} = 1:2 (see Figure S1 in the Supporting Information), implying the coordination between vesicles and Fe^{2+} ions. Transmission electron microscopy (TEM) observation and dynamic laser scattering (DLS) in Figure 1 A, 1B and S2 revealed that Fe^{2+}@vesicle had well-defined vesicular structure with an average radius of 25 nm. Atomic force microscopic (AFM) image showed that Fe^{2+}@vesicle was spherical particle, and the present concave feature confirmed the vesicular structure of Fe^{2+}@vesicle (Figure S3). Considering the collapsed structure in AFM image, the thickness of the vesicular membrane was half of the measured height from their AFM image (Figure S3), which were calculated to be ≈10.1 nm and 7.5 nm. Since the molecular lengths of TPE-BPA and CTAB were respectively calculated to be around 2.5 nm and 2.0 nm, the vesicle-like structures might possess a multilayer structure, where TPE-BPA acted as the framework of membrane. Similarly, after addition of the same amount of Fe^{3+} into TPE-BPA@8CTAB vesicle solution, Fe^{3+}@vesicle showed vesicular structure as well (Figure 1 C and S2), and AFM image also demonstrated the collapsed vesicular structure (Figure S4). In addition, the average radius and Zeta potential of Fe^{3+}@vesicles were 54 nm (Figure 1 A) and 3 mV (Figure 1 F), respectively.

Despite Fe^{2+}@vesicle and Fe^{3+}@vesicle showed identical vesicular structures, their differences in size distribution and Zeta potentials inspired us to modulate their reversible transformation via redox treatment. By bubbling O_2 to the Fe^{2+}@vesicle, the UV absorption at 462 nm that was the specific coordination characteristic between Fe^{2+} and coordinating group of TPE-BPA gradually decreased (Figure 1 D), suggesting the disappearance of this coordination,[10] which was also confirmed by the color change of solution from dark yellow to colorless. X-ray photoelectron spectroscopy (XPS) measurement further showed that the Fe^{2+} has been oxidized into Fe^{3+} (Figure S5). Additionally, upon bubbling O_2 to the Fe^{2+}@vesicle, the Zeta potentials of vesicles decreased from 25 mV to 5 mV, accompanied with an increase of vesicular radius from 25 nm to 54 nm (Figure 1 F). Meanwhile, TEM observation revealed that the vesicles obtained from oxidation had exactly the same structure as those directly prepared from Fe^{3+} (Figure S6A). These results definitely demonstrated that Fe^{2+}@vesicle was transformed into Fe^{3+}@vesicle. On the other hand, with addition of reductive Vitamin C (VC) to Fe^{3+}@vesicle system, UV absorption at 462 nm increased gradually, indicating the appearance of coordination between Fe^{2+} and TPE-BPA (Figure 1 E). Simultaneously, all the Zeta potentials, size of vesicles and the morphology of these generated vesicles were the same as the Fe^{2+}@vesicles (Figure 1 F and S6B), which strongly suggested that Fe^{3+}@vesicle was reduced to Fe^{2+}@vesicle by VC. Furthermore, the redox cycle between Fe^{2+}@vesicle and Fe^{3+}@vesicle can be reproduced for many times, which was witnessed by the alternative changes of both Zeta potential and size of the vesicle (Figure 1 G). As depicted by the TEM and AFM image (Figure S7), the vesicular morphology always remained constant during the repeated cycles. Combining all the results above, it seemed reasonable to infer that the transformation between Fe^{2+}@vesicle and Fe^{3+}@vesicle could be reversibly and controllably achieved by redox reaction.

Given that the original TPE-BPA@CTAB vesicle was nearly charge-neutral, it was understandable that binding of Fe^{2+} would increase the zeta potential of vesicle. However, it was rather surprising that binding of Fe^{3+}, which carried higher charges than Fe^{2+}, didn't change the zeta potential of vesicle very much. This can be attributed to the hydrolysis of Fe^{3+} ions under the experimental condition (pH 6). Indeed, theoretical analysis indicated that under the experimental pH condition, around 78 % Fe^{3+} existed in the form of non-charged $Fe(OH)_3$ while the 21 % was in the form of $Fe(OH)_2^+$ and 1 % was $Fe(OH)^{2+}$ (Figure S8). Since the hydrolyzed species $Fe(OH)_n^{(3-n)+}$ had weaker binding ability to the TPE-BPA vesicle, only few Fe^{3+} species were coordinated to increase the charges of Fe^{3+}@vesicle. This was proved by identical size and Zeta potential results between Fe^{3+}@vesicle and original vesicle (Figure S9), as well as the unchanged UV absorption (Figure S10). However, at the same pH 6 condition, Fe^{2+} was not hydrolyzed at all. Thus, a large amount of Fe^{2+} ions were located in Fe^{2+}@vesicle.

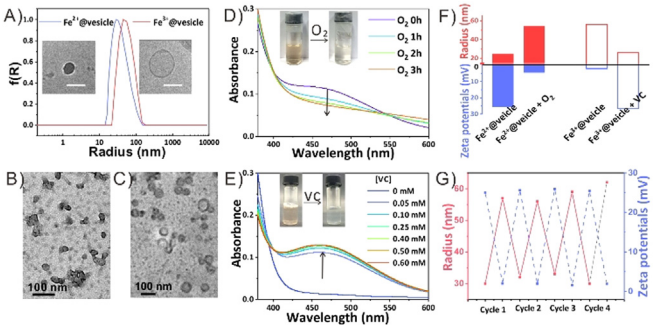

Figure 1. A) DLS results of Fe^{2+}@vesicles and Fe^{3+}@vesicles. Inserted pictures are Cryo-TEM images of Fe^{2+}@vesicles and Fe^{3+}@vesicles. Scale bar is 100 nm. TEM images of stained B) Fe^{2+}@vesicles and C) Fe^{3+}@vesicles. UV spectra of D) Fe^{2+}@vesicles upon exposure to O_2 and E) Fe^{3+}@vesicles with addition of VC. F) Radius and Zeta potentials variation of Fe^{2+}@vesicles upon exposure to O_2 and Fe^{3+}@vesicles with addition of VC. G) Reversible size and charged state change of the Fe^{2+}@vesicles upon the alternate addition of VC and O_2.

The redox reaction and hydrolysis could slow down the transformation, which provided opportunities to investigate the reversible processes. Real-time DLS measurement demonstrated that the scattered light intensity gradually decreased when sustaining bubbling O_2 into Fe^{2+}@vesicle solutions, which accompanied with gradual enlargement of the radius of vesicles over time (Figure 2A and B). The scattered light intensity is proportional to the number density and particle size of vesicles, therefore, the decrease of scattered intensity and increase of particle size would cause a significant reduce of number density of particles. This suggested that small vesicles may fuse into large vesicles during the oxidizing process. The fusion process was confirmed by TEM images where some small vesicles were fusing to form large beadlike structures (Figure 2C). Similarly, when VC was added into Fe^{3+}@vesicle solution, the scattered light intensity gradually increased over time and reached a platform within 25 min, simultaneously a decrease of vesicles size occurred (Figure 2D and E). The abnormal increase of scattered intensity and decrease of vesicle size in the smaller Fe^{2+}@vesicle system could be mainly ascribed to the growth of particle population, implying that fission behavior might occur in the reduction process. Interestingly, TEM images clearly demonstrated the fission that a small vesicle was budding from the large vesicle (Figure 2F).

The possible mechanism of reversible and controllable fusion and fission behaviors was illustrated in Figure 2G. In Fe^{2+}@vesicle, due to the strong electrostatic repulsive interaction of positively charges produced by coordination of Fe^{2+} ions, TPE-BPA molecules tended to repel each other and stacked in loose states. As a result, the vesicles possessed a large curvature in membrane and a small radius. When the Fe^{2+} was oxidized to Fe^{3+} by O_2, positive charges and electrostatic repulsive force drastically weakened, resulting in the compact stacking of vesicle membrane because most of the Fe^{3+} ions were hydrolyzed and the yielded hydrates showed negligible coordinated capacity. Consequently, vesicles fused together to lower their interaction free energy and formed large-sized vesicles with small curvature. Inversely, upon the reduction by adding VC, Fe^{3+} and their hydrates were transformed to Fe^{2+} ions, which held an excellent coordinated capacity to vesicles. The increased electrostatic repulsive force could cause the fission of vesicles, and subsequently generated small-sized vesicles with large curvature. Thus, the vesicles reverted back to their original state in the fission process via reduction. To check the dominant role of charges on fission and fusion of vesicles, Edetate disodium (EDTA) that had stronger coordination capability with Fe^{2+} than TPE-BPA was employed to remove metal ions. With stepwise addition of EDTA into Fe^{2+}@vesicle solution, the fluorescence of the vesicles gradually increased (Figure 3A), which suggested that Fe^{2+} ions were removed from vesicle because Fe^{2+} was able to quench the fluorescent emission. Moreover, the increase of radius and decrease of Zeta potentials of vesicles upon the addition of EDTA also demonstrated the vesicle fusion caused by the removal of charges (Figure S11). When 0.25 mM EDTA was added, the vesicles showed the same Zeta potential, radius and morphology as TPE-BPA@CTAB vesicles (Figure 3B), indicating that Fe^{2+}@vesicle recovered to the original uncoordinated vesicles.

Supramolecular materials based on AIE molecules display strong fluorescent emission, and the change of fluorescence is usually related to the rearrangement of AIE molecules.[11] This provides us a convenient and sensitive protocol to monitor the molecular packing architecture during vesicular transformation. Because of the inherent obstacles of fluorescence quenching caused by both Fe^{2+} and Fe^{3+} ions, Co^{2+} ions were utilized for the evaluation. TPE-

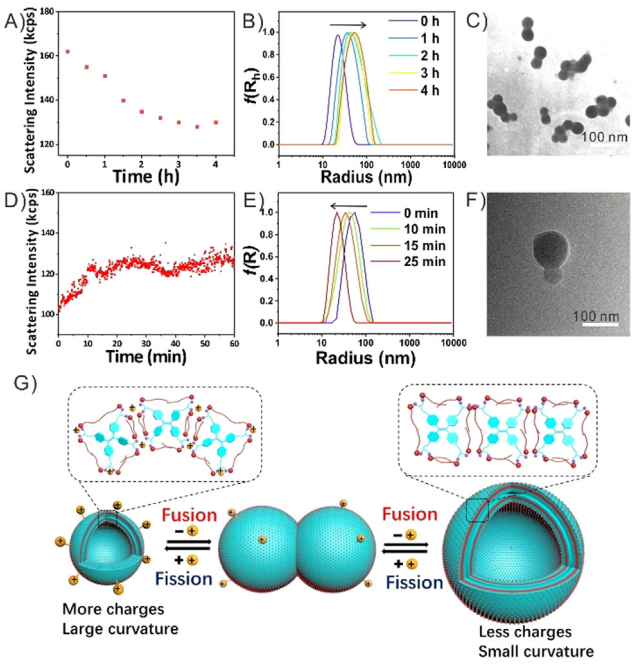

Figure 2. A) Real-time scattering intensity change and B) size distribution of Fe^{2+}@vesicles exposed to O_2. C) TEM images of fusion behaviors of Fe^{2+}@vesicles upon oxidation. D) Real-time scattering intensity change and E) size distribution of Fe^{3+}@vesicles with VC. F) TEM images of fission process of Fe^{3+}@vesicles upon reduction. G) Schematic illustration of possible mechanism of reversible and controllable fusion and fission behaviors.

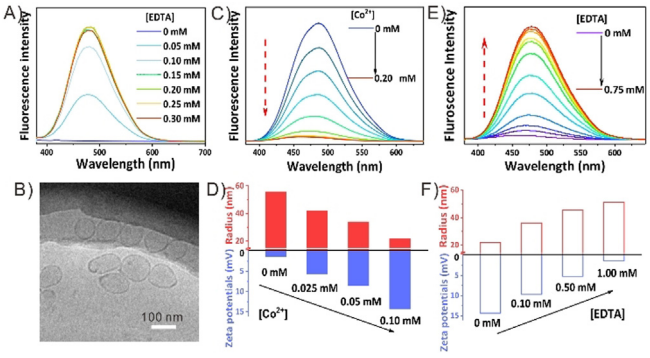

Figure 3. A) Fluorescence spectra of Fe^{2+}@vesicles with addition of EDTA. B) Cryo-TEM image of Fe^{2+}@vesicles with 0.25 mM EDTA. C) Fluorescence spectra and D) Zeta potentials-radius changes of vesicles with gradual addition of Co^{2+}. E) Fluorescence spectra and F) Zeta potentials-radius variation of Co^{2+}@vesicles with gradual addition of EDTA.

BPA@8CTAB vesicle was a charge-neutral vesicle with strong fluorescent emission. The stepwise addition of Co^{2+} ions induced the decrease in size of vesicles and the increase in Zeta potentials, corresponding to fission process caused by charges (Figure 3D). Meanwhile, a gradual decrease of fluorescent emission was observed, accompanying with a blue shift from 486 nm to 455 nm (Figure 3C). These results indicated that AIE molecules possessed a more and more twisted configuration and stacked loosely to each other in fission process. On the contrary, when EDTA was added to Co^{2+}@vesicles solution to remove the charges in membrane, both increased size and decreased Zeta potentials were determined, implying the occurrence of vesicle fusion (Figure 4F). Moreover, the fluorescent emission gradually increased with a red emission shift from 455 nm to 488 nm (Figure 4E), indicating that AIE molecules became more intensive during the fusion process. Combined with TEM images (Figure S12), these results further confirmed the supposed mechanism towards fusion and fission behaviors of the vesicles.

Biomolecules with critical role in living systems could be encapsulated in exosomes and transferred into cells, which stimulated us to take the exosome-mimetic vesicles as drug delivery. As one of the most promising agents for cancer therapy, siRNA plays important role in repairing the destroyed biosystems. However, efficient delivery is generally required because of the extremely low cellular uptake of siRNA.[12] Benefiting from the negatively charged feature of siRNA, positive Fe^{2+}@vesicle is potentially powerful as nanocarrier for siRNA. Upon the addition of siRNA into Fe^{2+}@vesicle solution, the Zeta potential decreased from 25 mV to −5 mV, solidly suggesting the binding of siRNA to vesicles (Figure S13). To straightforwardly track the cellular uptake of siRNA, red-emissive dye Cy5 was used to label siRNA. As depicted in S14, negligible fluorescent signal was observed in cells when free siRNA without vesicles was incubated in the cell culture. On the contrary, the cells exhibited bright emission after incubating siRNA-loaded Fe^{2+}@vesicle (siRNA@vesicle) for the same period. These outcomes obviously revealed that the utilization of Fe^{2+}@vesicle indeed promoted the delivery of siRNA to cells. Co-location images (Figure 4A and S15) further showed that siRNA was distributed in cytoplasm, and the overlap between siRNA and lysosome suggested that siRNA was effectively taken up by HeLa cells through endocytosis of siRNA@vesicle and then released into the cytoplasm. The release maybe ascribed to the oxidative intracellular environment of cancer cells[13] where the cell-engulfed Fe^{2+}@vesicle can be oxidized to Fe^{3+}@vesicle by the abundance of H_2O_2 in cancer cells, and the resulted decrease of positive charges weakened the interaction with siRNA. The Agarose gel electrophoresis results showed that siRNA was indeed released in the presence of H_2O_2 (Figure S16). Furthermore, the therapeutic efficiency of siRNA@vesicle was investigated by quantitatively evaluating on HeLa cancer cells. The study of dose-dependent cytotoxicity revealed that cancer cell viability was gradually and rapidly decreased with raising the concentration of siRNA@vesicle (Figure S15B). These results demonstrated that Fe^{2+}@vesicles were considerably potential candidates for siRNA delivery.

We have successfully fabricated an exosome-mimetic vesicle with reversible fusion and fission behaviors that could be controlled by redox. The charges of vesicle played a significant role in vesicular transformation. When Fe^{2+} was oxidized to Fe^{3+}, positive charges were removed from vesicle because the hydrolysis of Fe^{3+} ions decreased their coordinated capacity. Consequently, vesicles tended to fuse together and formed large-sized vesicles to lower the intension free energy. Inversely, upon reduction of Fe^{3+} to Fe^{2+}, the charges recovered and the enhanced electrostatic repulsive force led to the formation of small-sized vesicles through fission process. Moreover, benefiting from the AIE features of the vesicle building blocks, the molecular packing states in vesicular transformation were monitored by fluorescence emission changes. This study would thus provide innovative understanding for the fusion and fission behaviors of exosomes. Additionally, different from the traditional "breakdown" ways of releasing drugs, the exosome-mimetic vesicles release the loaded siRNA through fusion process, which provide us a new candidate for drug delivery system.

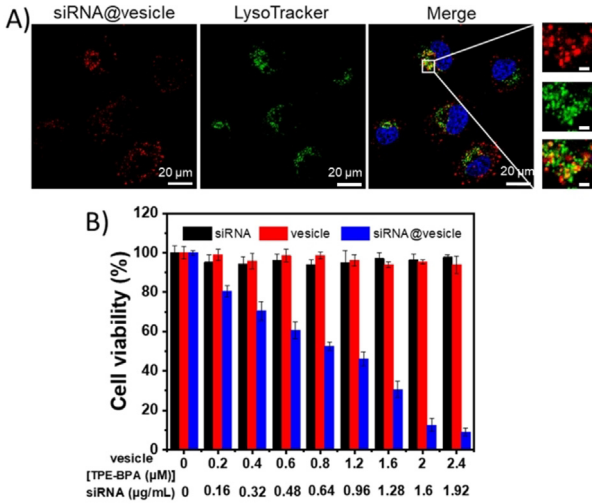

Figure 4. A) Co-location images of Hela cells after incubation with siRNA@vesicles for 4 h. SiRNA was labelled with Cy5 (red emission), lysosomes were stained by LysoTracker with green emission, and cell nucleus were stained by Hoechst with blue emission. Scale bar in magnified pictures is 2 μm. B) Cell viability of free siRNA, vesicle and siRNA@vesicle in Hela cells. The molar ratio of TPE-BPA, CTAB and Fe^{2+} in vesicle was 1:8:2, and the concentrations of vesicle were calculated by the concentration of TPE-BPA.

Acknowledgements

This work was financially supported by China Postdoctoral Science Foundation (Grant No. 2019M653005), the National Natural Science Foundation of China (Grant No. 21801169, 21902106), the Natural Science Foundation for Distinguished Young Scholars of Guangdong Province (2020B1515020011), and the Science and Technology Foundation of Shenzhen City (JCYJ20190808153415062).

Conflict of interest

The authors declare no conflict of interest.

Keywords: aggregation · fluorescence · nanostructures · supramolecular chemistry · vesicles

[1] a) L. Alvarez-Erviti, Y. Seow, H. Yin, C. Betts, S. Lakhal, M. J. A. Wood, *Nat. Biotechnol.* **2011**, *29*, 341 – 345; b) X. Zhou, F. Xie, L. Wang, L. Zhang, S. Zhang, M. Fang, F. Zhou, *Cell. Mol. Immunol.* **2020**, *17*, 323 – 334; c) Z. G. Zhang, B. Buller, M. Chopp, *Nat. Rev. Neurol.* **2019**, *15*, 193 – 203; d) A. Becker, B. K. Thakur, J. M. Weiss, H. S. Kim, H. Peinado, D. Lyden, *Cancer Cell* **2016**, *30*, 836 – 848.

[2] a) M. P. Bebelman, P. Bun, S. Huveneers, G. van Niel, D. M. Pegtel, F. J. Verweij, *Nat. Protoc.* **2020**, *15*, 102 – 121; b) C. Théry, M. Ostrowski, E. Segura, *Cell. Mol. Immunol.* **2009**, *9*, 581 – 593; c) T. Tian, Y. Wang, H. Wang, Z. Zhu, Z. Xiao, *J. Cell. Biochem.* **2010**, *111*, 488 – 496.

[3] a) E. van der Pol, A. N. Böing, P. Harrison, A. Sturk, R. Nieuwland, *Pharmacol. Rev.* **2012**, *64*, 676 – 705; b) C. Subra, D. Grand, K. Laulagnier, A. Stella, G. Lambeau, M. Paillasse, P. De Medina, B. Monsarrat, B. Perret, S. Silvente-Poirot, M. Poirot, M. Record, *J. Lipid Res.* **2010**, *51*, 2105 – 2120.

[4] a) J. C. Shillcock, R. Lipowsky, *Nat. Mater.* **2005**, *4*, 225 – 228; b) B. Gong, B.-K. Choi, J.-Y. Kim, D. Shetty, Y. H. Ko, N. Selvapalam, N. K. Lee, K. Kim, *J. Am. Chem. Soc.* **2015**, *137*, 8908 – 8911; c) N.-N. Deng, M. Yelleswarapu, L. Zheng, W. T. S. Huck, *J. Am. Chem. Soc.* **2017**, *139*, 587 – 590; d) J. Steinkühler, R. L. Knorr, Z. Zhao, T. Bhatia, S. M. Bartelt, S. Wegner, R. Dimova, R. Lipowsky, *Nat. Commun.* **2020**, *11*, 905; e) W. Zong, S. Ma, X. Zhang, X. Wang, Q. Li, X. Han, *J. Am. Chem. Soc.* **2017**, *139*, 9955 – 9960; f) T. Litschel, B. Ramm, R. Maas, M. Heymann, P. Schwille, *Angew. Chem. Int. Ed.* **2018**, *57*, 16286 – 16290; *Angew. Chem.* **2018**, *130*, 16522 – 16527.

[5] a) Y. Lyn, D. Cui, J. Huang, W. Fan, Y. Miao, K. Pu, *Angew. Chem. Int. Ed.* **2019**, *58*, 4983 – 4987; *Angew. Chem.* **2019**, *131*, 5037 – 5041; b) W. Nie, G. Wu, J. Zhang, L.-L. Huang, J. Ding, A. Jiang, Y. Zhang, Y. Liu, J. Li, K. Pu, H.-Y. Xie, *Angew. Chem. Int. Ed.* **2020**, *59*, 2018 – 2022; *Angew. Chem.* **2020**, *132*, 2034 – 2038.

[6] a) I. M. Henderson, W. F. Paxton, *Angew. Chem. Int. Ed.* **2014**, *53*, 3372 – 3376; *Angew. Chem.* **2014**, *126*, 3440 – 3444; b) S. Varlas, R. Keogh, Y. Xie, S. L. Horswell, J. C. Foster, R. K. O'Reilly, *J. Am. Chem. Soc.* **2019**, *141*, 20234 – 20248.

[7] a) J. Mei, N. L. C. Leung, R. T. K. Kwok, J. W. Y. Lam, B. Z. Tang, *Chem. Rev.* **2015**, *115*, 11718 – 11940; b) J. Li, J. Wang, H. Li, N. Song, D. Wang, B. Z. Tang, *Chem. Soc. Rev.* **2020**, *49*, 1144 – 1172.

[8] J. Li, K. Shi, M. Drechsler, B. Z. Tang, J. Huang, Y. Yan, *Chem. Commun.* **2016**, *52*, 12466 – 12469.

[9] a) Y. Yan, A. de Keizer, M. A. Cohen Stuart, N. A. M. Besseling, *Soft Matter* **2009**, *5*, 790 – 796; b) L. Xu, L. Jiang, M. Drechsler, Y. Sun, Z. Liu, J. Huang, B. Z. Tang, Z. Li, M. A. Cohen Stuart, Y. Yan, *J. Am. Chem. Soc.* **2014**, *136*, 1942 – 1947; c) Y. Lan, L. Xu, Y. Yan, J. Huang, A. de Keizer, N. A. M. Besseling, M. A. Cohen Stuart, *Soft Matter* **2011**, *7*, 3565 – 3570.

[10] Y. Yan, Y. Lan, A. Keizer, M. Drechsler, H. V. As, M. C. Stuart, N. A. M. Besseling, *Soft Matter* **2010**, *6*, 3244 – 3248.

[11] a) K. Li, Y. Lin, C. Lu, *Chem. Asian J.* **2019**, *14*, 715 – 729; b) W. Guan, W. Zhou, C. Lu, B. Z. Tang, *Angew. Chem. Int. Ed.* **2015**, *54*, 15160 – 15164; *Angew. Chem.* **2015**, *127*, 15375 – 15379; c) Z. Wang, J. Nie, W. Qin, Q. Hu, B. Z. Tang, *Nat. Commun.* **2016**, *7*, 12033; d) J. Liang, B. Z. Tang, B. Liu, *Chem. Soc. Rev.* **2015**, *44*, 2798 – 2811; e) Z. Wang, X. He, T. Yong, Y. Miao, C. Zhang, B. Z. Tang, *J. Am. Chem. Soc.* **2020**, *142*, 512 – 519.

[12] a) F. Ding, Q. Mou, Y. Ma, G. Pan, Y. Guo, G. Tong, C. H. J. Choi, X. Zhu, C. Zhang, *Angew. Chem. Int. Ed.* **2018**, *57*, 3064 – 3068; *Angew. Chem.* **2018**, *130*, 3118 – 3122; b) M. Zheng, T. Jiang, W. Yang, Y. Zou, H. Wu, X. Liu, F. Zhu, R. Qian, D. Ling, K. McDonald, J. Shi, B. Shi, *Angew. Chem. Int. Ed.* **2019**, *58*, 4938 – 4942; *Angew. Chem.* **2019**, *131*, 4992 – 4996; c) O. S. Fenton, K. J. Kauffman, R. L. McClellan, J. C. Kaczmarek, M. D. Zeng, J. L. Andresen, L. H. Rhym, M. W. Heartlein, F. D. Rosa, D. G. Anderson, *Angew. Chem. Int. Ed.* **2018**, *57*, 13582 – 13586; *Angew. Chem.* **2018**, *130*, 13770 – 13774.

[13] a) B. Kumar, S. Koul, L. Khandrika, R. B. Meacham, H. K. Koul, *Cancer Res.* **2008**, *68*, 1777 – 1785; b) T. P. Szatrowski, C. F. Nathan, *Cancer Res.* **1991**, *51*, 794 – 798.

Manuscript received: July 27, 2020
Accepted manuscript online: August 10, 2020
Version of record online: September 17, 2020

